



Cite this: *Nanoscale*, 2015, 7, 12018

Dynamically configurable hybridization of plasmon modes in nanoring dimer arrays†

Lei Zhang,^{*a} Zhaogang Dong,^b Ying Min Wang,^b Yan Jun Liu,^b Shuang Zhang,^c Joel Kwang Wei Yang^{b,d} and Cheng-Wei Qiu^{*a,e}

We present a novel strategy capable of dynamically configuring the plasmon-induced transparency (PIT) effect with a polarization-dependent controllability based on a nanoring dimer array. The controllable coupling strength between the superradiant and subradiant modes is due to the polarization-dependent field distributions. It is shown that this dynamically controlled PIT is realized with a modulation depth as high as 95%, and a linear dependence of the coupling strength on polarization angle is deduced using a coupled-oscillator model. We believe that our results will inspire further exciting achievements that utilize various polarization states of the electromagnetic wave and pave a way towards applications using PIT with dynamic controllability such as slow light, optical nonlinearities and chemical/bio-sensing.

Received 11th May 2015,
Accepted 13th June 2015

DOI: 10.1039/c5nr03094c

www.rsc.org/nanoscale

Introduction

Fano resonance, which results from hybridizing a broadband superradiant and a narrowband subradiant mode,^{1,2} has drawn great interest due to its versatility in near-field control^{3,4} and far-field response.⁵ A myriad of applications of Fano resonance have been explored such as sensing,^{6,7} plasmonic trapping,⁸ and nonlinear optical effect enhancement.^{9,10} As a special case, the plasmon-induced transparency (PIT) resulting from the coupling of two slightly detuned modes has been demonstrated by stacking a metallic nanorod, providing a broadband mode on a pair of metallic nanowires, acting as a narrowband mode, either horizontally or vertically.^{11,12} However, due to the anisotropic electromagnetic response of the building blocks, previous demonstrations have lacked dynamical controllability because the coupling between two resonances is dependent on their relative separation, which is

fixed for a given design. It is thus challenging to achieve dynamically controlled transparency with the existing designs.

Here, we would like to emphasize that the essence of coupling lies on the spatial overlap of the field distributions, rather than merely the physical separation of the structures. Usually, the overlap area is enlarged by moving two structures towards each other. If this overlap area can be controlled with an alternative approach, the coupling strength can also be controlled. As one potential candidate, polarization is capable of rotating the corresponding field nodes of the respective modes so as to tune their coupling efficiency. However, there has not yet been a thorough investigation on the dynamic control of the PIT effect by tuning polarization, although polarization has been applied to dynamically engineer resonant modes for different applications such as plasmonic trapping and rotating.¹³ In particular, more polarization states have been realized such as radially and azimuthally polarized states. Therefore, it is of realistic significance to study the influence of polarization states on the resonant response of a system.

In this work, we propose a novel strategy to achieve dynamically controlled hybridization based on a dissimilar nanoring dimer.^{14–16} As a demonstration, a polarization-controlled PIT effect is investigated both numerically and experimentally. By rotating the polarization of incident light, the entire system can convert from opaque to transparent and *vice versa*, with a modulation depth as high as 95%. Furthermore, it is found that the coupling strength is approximately linearly proportional to the polarization angle, which opens up a novel mechanism for controlling mode interaction. Our proposed scheme expands the current understanding of mode coupling, which will inspire promising applications for nanoplasmonic devices with polarization-enabled controllability.

^aDepartment of Electrical and Computer Engineering, National University of Singapore, Singapore 117583. E-mail: elezlei@nus.edu.sg, eleqc@nus.edu.sg

^bInstitute of Materials Research and Engineering, Agency for Science, Technology and Research (A*STAR), Singapore 117602

^cSchool of Physics and Astronomy, University of Birmingham, Birmingham B15 2TT, UK

^dSingapore University of Technology and Design, Singapore 138682

^eSZU-NUS Collaborative Innovation Center for Optoelectronic Science and Technology, Shenzhen University, Guangdong 518060, China

†Electronic supplementary information (ESI) available: Method, mode supported by single nanoring, transmittance spectrum of single nanoring, comparison of transmittance spectra simulated under different illumination angles, diffraction coupling in the proposed nanoring dimer system, and the coupled Lorentz oscillator model and parameters fitting. See DOI: 10.1039/c5nr03094c

Results and discussion

The unit cell of the proposed design consists of two dissimilar nanorings separated by a small gap, as shown in Fig. 1a. A representative SEM image of the fabricated sample is taken at a tilted angle of 45° , as shown in Fig. 1b. The dimensions of the two nanorings were chosen carefully so that the resonances of the superradiant dipolar mode of the left nanoring and the subradiant quadrupolar mode of the right nanoring are closely aligned in frequency. As a reference, when there is only one left nanoring, a transmission dip in the first row in Fig. 1c arises from the strong absorption caused by exciting the superradiant mode, which is shown by the dipolar field distribution in the first row of Fig. 1d.

When a second nanoring supporting the superradiant mode is introduced at a separation of 10 nm, the change in transmittance is negligible when the polarization angle is perpendicular to the x -axis, *i.e.* $\varphi = 90^\circ$, as shown in the second row of Fig. 1c. In this case, the quadrupolar mode cannot be excited by far field or by near field. The former can be attributed to the lack of a net dipole moment under normal incidence. On the other hand, the latter is due to the fact that the antinodes of the dipolar field are far away from the antinodes

of the quadrupolar mode, as shown in the second row of Fig. 1d. As a result, negligible coupling exists between them and no perceivable difference in the field distributions was found. When the polarization is rotated in a clockwise manner, one antinode of the dipolar field gradually approaches the quadrupolar field antinodes. Their coupling strength increases, resulting from their energy exchange. With this exchange, partially destructive interference between the two pathways exciting the superradiant mode weakens the coupling of incident energy into the system and leads to an increase in transmission, while the electric field starts to distribute around the right nanoring. When the electric field is polarized along the x -axis, *i.e.* $\varphi = 0^\circ$, the field antinodes are aligned to achieve the maximum coupling strength. This effect, in turn, maximizes the destructive interference, and the entire system becomes transparent with a transmittance of 0.72, which is considerably higher than the transmittance of 0.036 supported when $\varphi = 90^\circ$. Simultaneously, the electric field is mainly confined around the right nanoring, resulting in a quadrupolar distribution, while the dipolar field distribution of the left nanoring disappears, which leads to an inefficient absorption of the incident optical field and thus a high transmittance. The resultant modulation depth, defined as $|(T_{\text{on}} - T_{\text{off}})/T_{\text{on}}| \times 100\%$, reaches as high as 95%, where T_{on} and T_{off} represent the transmittance with the maximized PIT and without PIT effect, respectively. It should be pointed that the field distributions of the dipolar and quadrupolar modes of the nanorings possess C_2 and C_4 symmetry, respectively. The field distribution of the quadrupolar mode remains the same under polarization at both $\varphi = 90^\circ$ and $\varphi = 0^\circ$. All the spectrum changes caused by polarization rotation arise from the rotation of dipolar mode, which is different from coupling between two dipolar modes.

The coupling strength between two superradiant modes using two identical nanoring dimers can be controlled by varying their separation distance, as discussed in the literature.^{17,18} However, to the best of our knowledge, the specific mode coupling controlled by polarization has yet to be discussed in the context of the interactions between the superradiant and the subradiant modes. Here, a small nanoring is chosen to support a superradiant mode with a resonance frequency of 285.4 THz. The full-width at half-maximum (FWHM) is 26.1 THz, as obtained by fitting the transmittance spectrum with a Lorentzian function. The transmission dip will flip over as a peak when a larger nanoring supporting subradiant mode is placed on its right side. The difference in the dip and peak positions could be attributed to the slight mismatch between the resonance frequencies of two modes, which coincide with each other as d_2 reaches 300 nm, as shown in Fig. 2a.

The strong coupling between the superradiant and subradiant modes can be understood with a typical three-level system, as shown in Fig. 2b.^{12,19,20} $|0\rangle$ represents the ground state; $|1\rangle$ and $|2\rangle$ are the excited states, which represent the superradiant mode and subradiant mode, respectively. The field distributions of the E_z component shown in Fig. 2b and c are plotted at a plane 2 nm above the structure surface, indicating

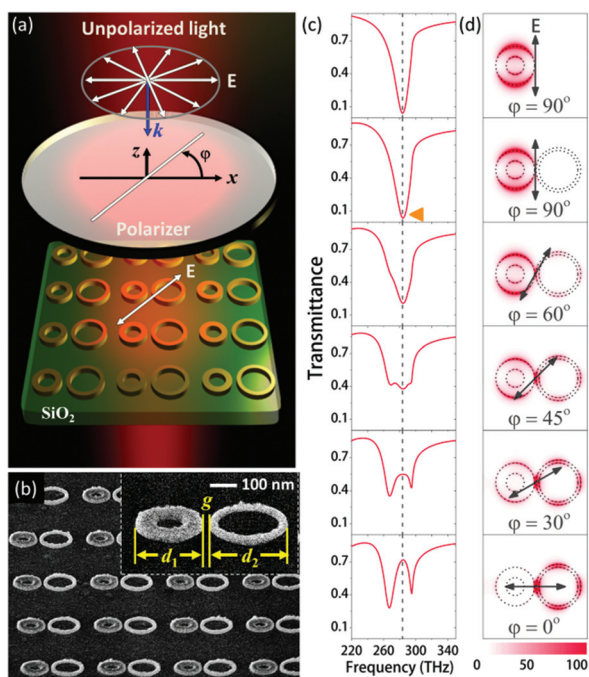


Fig. 1 (a) Schematic of the proposed structure. (b) Angled-view scanning electron micrograph (SEM) of the sample fabricated by electron beam lithography (EBL) showing an array of nanoring dimers. (c) Simulated transmittance spectra under illumination with different polarization angles. Diameters $d_1 = 260$ nm and $d_2 = 300$ nm. (d) Electric field intensity distribution at a plane 2 nm above the structures at the frequency 285.4 THz, as indicated by the dashed line in column (c). For all the simulations: the height of the nanoring is 40 nm; the gap g is 10 nm; the periodicity is 700 nm; the wall thicknesses of the left and right nanorings are 70 nm and 20 nm, respectively.

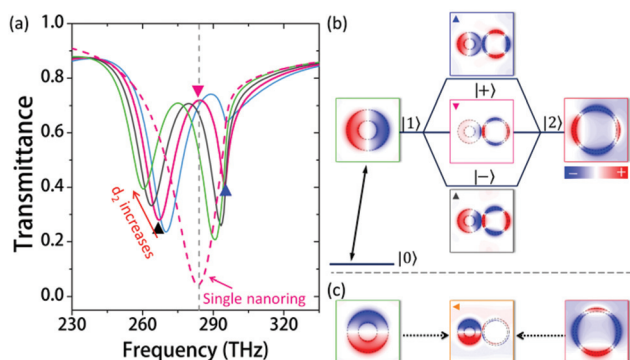


Fig. 2 (a) Transmittance evolves as the diameter d_2 increases from 290 nm to 320 nm with a step of 10 nm, where diameter $d_1 = 260$ nm and the wall thicknesses of the left and right nanorings are 70 nm and 20 nm, respectively; polarization angle $\varphi = 0^\circ$. The transmittance of a single nanoring with diameter $d = 260$ nm is plotted as a reference, indicated by the dashed line. (b) Field distribution of the E_z component under excitation with a polarization angle of $\varphi = 0^\circ$, indicating a strong coupling. (c) Field distribution of the E_z component under excitation with a polarization angle of $\varphi = 90^\circ$, indicating a weak coupling. Field distributions are calculated under normal illumination except for quadrupolar mode, simulated with an incident angle of 30° .

the corresponding surface charge distributions.²¹ Under far-field excitation, $|0\rangle \rightarrow |1\rangle$ is a dipole-allowed transition, while $|0\rangle \rightarrow |2\rangle$ is a dipole-forbidden transition under normal incidence. However, it becomes allowable under inclined illumination due to the retardation effect, indicated by a distorted quadrupolar field distribution, as shown in Fig. 2b. In addition to far-field excitation, near-field coupling is another way to excite the subradiant mode. When the superradiant mode is in close proximity to the subradiant one, the strong near-field of $|1\rangle$ could excite $|2\rangle$ and *vice versa*. As a result, there exist two pathways to excite the superradiant mode, *i.e.* $|0\rangle \rightarrow |1\rangle$ and $|0\rangle \rightarrow |1\rangle \rightarrow |2\rangle \rightarrow |1\rangle$. When they interfere destructively, the dipolar field almost diminishes, which is obviously exhibited by the field distribution, as labelled by a pink-downward triangle in Fig. 2b. Therefore, both the reflection and absorption can be extremely suppressed, and the entire system will become transparent to give rise to the PIT effect.

Concomitantly, two sharp transmission dips originate from the coupling between $|1\rangle$ and $|2\rangle$. From the perspective of mode hybridization, the original energy state splits into two hybridized modes with one at high frequency $|+\rangle$ and the other at low frequency $|-\rangle$. As a result, a band gap opens up at the original frequency, which results in a transparent window due to inefficient light absorption. In this sense, the PIT effect could be considered as a byproduct of mode hybridization. It is remarkable that the FWHM of the lower frequency resonance is only 16.6 THz, which is even smaller than the Drude damping limit of Rayleigh nanoparticles (18 THz).²² Generally, for a given system, the decay rate of a mode is determined by the ratio of the volume of the conductor into which the fields penetrate because of the finite conductivity over the volume

occupied by the fields. This indicates that the decay properties of a mode could be tuned by distorting its field distribution,²³ which has been verified in ref. 12. In our case, the reduction in decay rate arises from the effective suppression of the radiative dissipation as well as the intrinsic absorption. The latter is mainly caused by a significant amount of electric field spreading out of the metallic parts during the circulation of energy between two nanorings. The energy ratio absorbed by the metallic part is only 41% at 267.4 THz, which is also smaller than the counterpart of Rayleigh particles, *i.e.* 57%.²² Furthermore, it is found that there is no energy flow between the neighbouring unit cell, as shown in the ESI.† Therefore, the narrow peaks observed in our proposed system must result from the energy decay within one unit cell. On the other hand, the linewidth of the higher frequency mode is only 10.4 THz. Both the localized coupling between the superradiant–subradiant modes and the diffraction effect contribute to this drastically narrow linewidth.^{6,24,25} It is thus implied that this compound system provides an efficient approach to decelerate the dissipation process of plasmon, which has great potential for applications such as sensing, light emission, and solar cells.

From a system perspective, two nanorings can be deemed as a whole. As a result, the final mode of the system should result from the interplay of two fundamental modes on each nanoring. The first and second modes, containing both obvious dipolar and quadrupolar field distributions, can be excited at the polarization angle $\varphi = 0^\circ$, as shown in Fig. 2b. They can differentiate from the π -phase difference between the fields at both sides of the gap. The third mode of the system is identified with the field distribution at a polarization angle of $\varphi = 90^\circ$, as shown in Fig. 2c, where the dipolar field is clearly rendered but the quadrupolar field is very weak. In this connection, there are three modes overall supported at the frequency range of interest. However, it is worth emphasizing that these three modes originate from the strong or weak coupling of dipolar and quadrupolar modes. In other words, the latter two modes are the essential cause of the phenomenon observed in this system. Therefore, to quantitatively explore coupling in a dissimilar nanoring dimer system, only two modes, *i.e.* the dipolar mode and the quadrupolar mode, are involved in the coupled Lorentz oscillator model.^{11,12,26} The amplitude of the superradiant dipolar mode A_1 can be obtained as

$$|A_1| = \left| \frac{\eta(-\omega + \omega_2 - i\gamma_2/2)}{(-\omega + \omega - i\gamma_2/2)(-\omega + \omega_2 - i\gamma_2/2) - \kappa^2} E_0 + \text{bg} \right| \quad (1)$$

which can interact with incoming light directly with a geometric factor η . The other oscillator, denoting the subradiant mode, can be excited through near-field coupling with a coupling strength of κ . γ_j is the damping rate. E_0 is the amplitude of the incident field. Since the incident energy is not perfectly coupled into the superradiant dipole mode, a constant field component bg should be taken into account as a background.^{8,27,28}

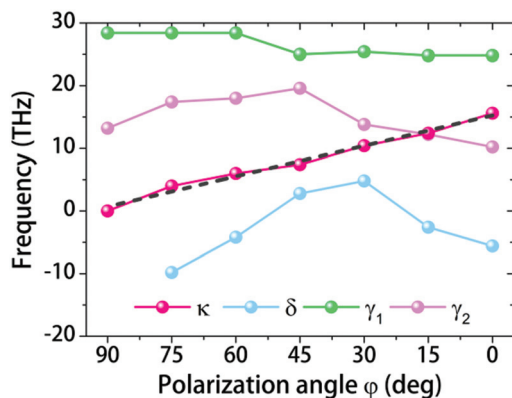


Fig. 3 Retrieved coupling and damping parameters against polarization angles. The black dashed line shows the linear fitting of the coupling strength against the polarization angle ϕ .

To unveil the interaction between two fundamental modes, the coupling and damping parameters can be obtained by fitting the magnitudes of the electric field with eqn (1). The retrieved parameters are plotted in Fig. 3. When the polarization angle ϕ is 90° , the fitted damping rate γ_1 of the super-radiant mode is 28.4 THz, which matches well with the value of the single dipolar mode by fitting with a Lorentzian function; the estimated damping rate γ_2 of the subradiant quadrupole mode is simply set to be 14.0 THz, which is obtained from inclined illumination of the single quadrupolar mode. κ is set as 0 due to a negligible coupling. Significantly, the coupling strength κ is approximately linearly proportional to the polarization angle, and it increases as the polarization angle decreases owing to a better alignment of field antinodes between the two modes; see a detailed discussion in the ESI.† This novel scheme for controlling mode coupling has great potential in plasmonic devices. Notably, there are also slight changes in the fitted decay rates, which may be beyond general consideration. Usually, as one of the intrinsic properties of a given mode, the decay rate is known as a constant. However, this statement may not be appropriate for a more general case when field distributions have distortions.²³ Due to the strong coupling, the field profiles around each nanoring deviate from the corresponding eigenmodes. Therefore, the observed decay rate may also include the contributions from other eigenmodes, which leads to a change in the decay rate. Accordingly, it is reasonable that the decay rate varies in our work; this variation results from the distortion of the fields caused by gradually rotating the polarization clockwise, as shown in Fig. 1d. Polarization-dependent excitation could thus provide a feasible approach to engineer the decay properties of plasmonic resonances. It should be noted that the coupled oscillator model provides a good explanation for the main features of the proposed system. However, the real system is considerably more complicated. For instance, the coupling strength could be a complex value instead of a real quantity when an additional phase factor is taken into account.²⁹

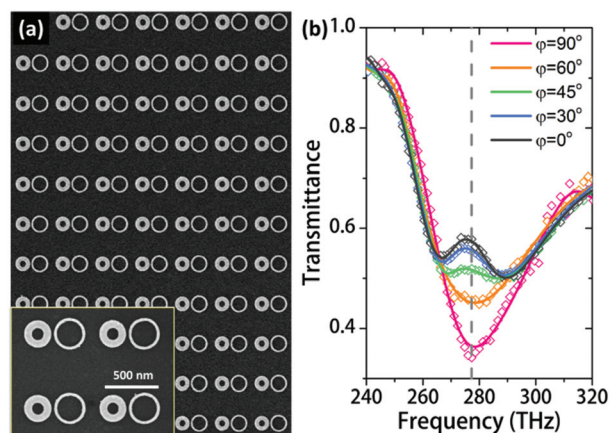


Fig. 4 (a) Top view of SEM image of the fabricated sample. Inset shows the close-up SEM image. $d_1 = 254$ nm, $d_2 = 300$ nm, $g = 20$ nm, and periodicity = 700 nm; the wall thicknesses of the two nanorings are 75 nm and 29 nm. (b) Transmittance spectra measured under illumination with different polarizations.

The proposed polarization-dependent PIT device was experimentally verified *via* the sample fabricated by EBL. As the polarization of incident light rotates from 90° to 0° , the transmittance increases from 0.34 to 0.58 at a frequency of 275.8 THz, as shown in Fig. 4b, reaching a maximum as the electric field oscillates along the center-to-center axis of the two nanorings. The modulation depth achieved experimentally is thus 41%, which is smaller than the 93.9% obtained in simulation with $g = 20$ nm. The difference between the theoretical calculation and the experimental measurement can be largely attributed to grain boundaries, large damping caused by the adhesion layer, and deviations from a perfect normal excitation. Nonetheless, the trends in our experimental findings support the validity of our theoretical predictions, clearly demonstrating the feasibility of polarization-based dynamic control of the PIT effect exhibited by the proposed nanoring dimer structure. Although polarization-dependent transparency has been investigated previously, the working mechanisms of these studies, relying either on the control of phase difference of two bright modes or on the turning on/off of the dark mode, are quite different from ours.^{30,31}

Conclusions

In summary, a novel strategy of realizing dynamically controllable hybridization of plasmon modes was proposed based on dissimilar nanoring dimer arrays. As a demonstration, the polarization-controlled PIT effect was investigated both numerically and experimentally. Through aligning the field antinodes of the superradiant mode with the subradiant mode by rotating polarization, the entire structure undergoes a transition from opaque to transparent. The modulation depth achieved was calculated to be as high as 95%. The coupling strength between the two modes is linearly proportional to the

polarization angle, as shown by a coupled oscillator model. Our proposed structure demonstrated a promising approach in controlling both near-field coupling and far-field response with dynamic tunability by simply controlling the incident polarization. Lastly, we believe that this dynamical manipulation strategy will inspire other exciting achievements utilizing polarization states of electromagnetic waves.

Acknowledgements

L.Z and C.-W.Q acknowledge the financial support from National University of Singapore (Grant No. R-263-000-A45-112). Z.D, Y.M.W and J.K.W.Y acknowledge the funding support from Agency for Science, Technology and Research (A*STAR) Young Investigatorship (Grant No. 0926030138), SERC (Grant No. 092154099), and National Research Foundation (Grant No. NRF-CRP 8-2011-07).

Notes and references

- 1 A. E. Miroshnichenko, S. Flach and Y. S. Kivshar, *Rev. Mod. Phys.*, 2010, **82**, 2257–2298.
- 2 B. Luk'yanchuk, N. I. Zheludev, S. A. Maier, N. J. Halas, P. Nordlander, H. Giessen and C. T. Chong, *Nat. Mater.*, 2010, **9**, 707–715.
- 3 J. Ye, F. Wen, H. Sobhani, J. B. Lassiter, P. V. Dorpe, P. Nordlander and N. J. Halas, *Nano Lett.*, 2012, **12**, 1660–1667.
- 4 S. Campione, C. Guclu, R. Ragan and F. Capolino, *ACS Photonics*, 2014, **1**, 254–260.
- 5 B. Gallinet and O. J. F. Martin, *ACS Nano*, 2011, **5**, 8999–9008.
- 6 L. Zhang, C. Y. Chan, J. Li and H. C. Ong, *Opt. Express*, 2012, **20**, 12610–12621.
- 7 Y. Zhan, D. Y. Lei, X. Li and S. A. Maier, *Nanoscale*, 2014, **6**, 4705–4715.
- 8 Z. Li, S. Zhang, L. Tong, P. Wang, B. Dong and H. Xu, *ACS Nano*, 2013, **8**, 701–708.
- 9 G. F. Walsh and L. Dal Negro, *Nano Lett.*, 2013, **13**, 3111–3117.
- 10 Y. Zhang, F. Wen, Y.-R. Zhen, P. Nordlander and N. J. Halas, *Proc. Natl. Acad. Sci. U. S. A.*, 2013, **110**, 9215–9219.
- 11 S. Zhang, D. A. Genov, Y. Wang, M. Liu and X. Zhang, *Phys. Rev. Lett.*, 2008, **101**, 047401.
- 12 N. Liu, L. Langguth, T. Weiss, J. Kastel, M. Fleischhauer, T. Pfau and H. Giessen, *Nat. Mater.*, 2009, **8**, 758–762.
- 13 K. Wang, E. Schonbrun, P. Steinvurzel and K. B. Crozier, *Nat. Commun.*, 2011, **2**, 469.
- 14 J. Aizpurua, P. Hanarp, D. S. Sutherland, M. Käll, G. W. Bryant and F. J. García de Abajo, *Phys. Rev. Lett.*, 2003, **90**, 057401.
- 15 Y. Cai, Y. Li, P. Nordlander and P. S. Cremer, *Nano Lett.*, 2012, **12**, 4881–4888.
- 16 H. Liu, E. S. P. Leong, Z. Wang, G. Si, L. Zheng, Y. J. Liu and C. Soci, *Adv. Opt. Mater.*, 2013, **1**, 978–983.
- 17 R. Near, C. Tabor, J. Duan, R. Pachter and M. El-Sayed, *Nano Lett.*, 2012, **12**, 2158–2164.
- 18 C.-Y. Tsai, J.-W. Lin, C.-Y. Wu, P.-T. Lin, T.-W. Lu and P.-T. Lee, *Nano Lett.*, 2012, **12**, 1648–1654.
- 19 M. Fleischhauer, A. Imamoglu and J. P. Marangos, *Rev. Mod. Phys.*, 2005, **77**, 633–673.
- 20 T. J. Davis, D. E. Gómez and K. C. Vernon, *Nano Lett.*, 2010, **10**, 2618–2625.
- 21 A. Lovera, B. Gallinet, P. Nordlander and O. J. F. Martin, *ACS Nano*, 2013, **7**, 4527–4536.
- 22 F. Wang and Y. R. Shen, *Phys. Rev. Lett.*, 2006, **97**, 206806.
- 23 J. D. Jackson, *Classical Electrodynamics*, John Wiley & Sons, New York, 1975.
- 24 V. G. Kravets, F. Schedin and A. N. Grigorenko, *Phys. Rev. Lett.*, 2008, **101**, 087403.
- 25 A. A. Yanik, A. E. Cetin, M. Huang, A. Artar, S. H. Mousavi, A. Khanikaev, J. H. Connor, G. Shvets and H. Altug, *Proc. Natl. Acad. Sci. U. S. A.*, 2011, **108**, 11784–11789.
- 26 S. Zhang, Z. Ye, Y. Wang, Y. Park, G. Bartal, M. Mrejen, X. Yin and X. Zhang, *Phys. Rev. Lett.*, 2012, **109**, 193902.
- 27 C. Ropers, D. J. Park, G. Stibenz, G. Steinmeyer, J. Kim, D. S. Kim and C. Lienau, *Phys. Rev. Lett.*, 2005, **94**, 113901.
- 28 A. Christ, Y. Ekinici, H. H. Solak, N. A. Gippius, S. G. Tikhodeev and O. J. F. Martin, *Phys. Rev. B: Condens. Matter*, 2007, **76**, 201405.
- 29 R. Taubert, M. Hentschel, J. Kästel and H. Giessen, *Nano Lett.*, 2012, **12**, 1367–1371.
- 30 J. Chen, P. Wang, C. Chen, Y. Lu, H. Ming and Q. Zhan, *Opt. Express*, 2011, **19**, 5970–5978.
- 31 W.-S. Chang, J. B. Lassiter, P. Swanglap, H. Sobhani, S. Khatua, P. Nordlander, N. J. Halas and S. Link, *Nano Lett.*, 2012, **12**, 4977–4982.